

How Concrete Filling Fundamentally Changes Stress-Strain Curve of Angle-Ply FRP Tubes in Tension

Akram Jawdhari¹, Amir Fam, FASCE² and Pedram Sadeghian, MASCE³

¹ Assistant Professor, Department of Civil Engineering, Valparaiso University, Valparaiso, IN 46383, USA and former Post-Doctoral Fellow at Queen's University, Canada.

² Donald and Sarah Munro Chair Professor and Associate Dean Research, Department of Civil Engineering, Queen's University, Kingston, ON, K7L 3N6, Canada, Email: amir.fam@queensu.ca (corresponding author)

³ Associate Professor and Canada Research Chair in Sustainable Infrastructure, Department of Civil and Resource Engineering, Dalhousie University, Halifax, NS, B3H 4R2, Canada.

ABSTRACT

Angle-ply ($\pm 55^\circ$) fiber reinforced polymer (FRP) tube is widely available and has been used in concrete-filled FRP tube (CFFT) members. Two observations have been reported regarding the behavior of this tube in tension: a remarkably nonlinear stress-strain response, and a significant increase in its tensile strength and stiffness when filled with concrete. To better understand these phenomena, a robust finite element model is developed using LS DYNA software and validated against a diverse experimental database. It showed that nonlinear behavior of the tube is mainly due to matrix cracking perpendicular to the fibers and to a lesser extent due to in-plane shear along diagonal bands. Concrete filling restrains the large radial and circumferential contraction of the hollow tube under longitudinal tension, thereby generates significant hoop tensile stresses and consequently a state of bi-axial tensile stress. Failure envelope under such stress combination was developed and far exceeded uniaxial strength in either direction. A parametric study was performed on 68 new models with various properties. The longitudinal tensile strength (σ_{max}) of CFFT tubes with fiber angles (θ) relative to longitudinal axis of 35, 45, 55, 65 and 75° increased 2.9, 4.1, 3.3, 2.8, and 1.4 times that of hollow counterparts. Design-oriented equations were developed to represent the enhanced longitudinal bi-linear stress-strain curve when the tube is filled with concrete. It can be used for flexural strength calculations of CFFTs, which would otherwise be grossly underestimated if calculated using hollow tube properties reported by manufacturer or established from longitudinal coupon tests or from Classical Lamination Theory.

Key words: GFRP tubes; angle-ply; tension; concrete; CFFT; FEA; LS DYNA; design model.

DOI: [https://doi.org/10.1061/\(ASCE\)CC.1943-5614.0001245](https://doi.org/10.1061/(ASCE)CC.1943-5614.0001245)

INTRODUCTION

Hollow fiber reinforced polymer (FRP) tubes and concrete-filled FRP tubes (CFFTs) are an attractive option for several structural applications. This includes piles, columns and girders using CFFTs; and poles for electric transmission, telecommunications, street lighting and overhead sign structures using hollow tubes or CFFTs (Ibrahim et al. 2000; Fam et al. 2003a,b; Mitchel and Fam 2010). FRP tubes are also commonly used in the pipeline industry (Ashraf et al. 2014; Rafiee 2016). The popular use of FRP tubes is particularly due to their light weight, leading to reductions in transportation and installation costs; and their corrosion resistance, making them ideal for harsh environments (Son and Fam 2008; Lu et al. 2020). In CFFTs, combining concrete infill and FRP tube produces a strong, corrosion-resistant, and ductile hybrid member, where the tube acts as a stay-in-place formwork and provides confinement, flexural and shear reinforcement, and protection against environmental effects; while the infill resists compressive forces and prevents local buckling of the tube (Mandal and Fam 2006; Xie et al. 2020).

Strength and stiffness of FRP tubes, which are mostly fabricated by the filament winding method, can be engineered by controlling the fiber angles, ratio of fibers in longitudinal and circumferential directions, and number of layers, to fit specific applications (Xie et al. 2020). Despite the endless possibilities, the tubes are commonly available in two general laminate structures; cross-ply, with layers mainly being oriented orthogonal to each other $[0/90^\circ]$ or close to; and angle-ply, with layers oriented at $\pm\theta^\circ$ angles relative to longitudinal axis. Although cross-ply tubes are more suitable for structural applications, angle-ply ones, particularly those with $\pm 55^\circ$, have been widely adopted for pressure pipes as will be discussed further (Shao and Mirmiran 2005;

Betts et al. 2019). While analyzing cross-ply composites is relatively simple and straightforward due to their nearly linear elastic behavior, angle-ply ones require special modeling due to their significant nonlinearities, which is the subject of this paper.

Angle-ply FRP tubes have been the subject of research for more than four decades, focusing mainly on their behavior as pipes carrying internal fluids. For example, Soden et al. (1993) performed testing on glass-FRP (GFRP) tubes, examining two parameters: winding angle (θ) and three cases of loading; axial (tension or compression), internal pressure, and bi-axial (pressure/axial). Similar tests were conducted by others (Carrol et al. 1995; Bai et al. 1997a,b) showing that tensile stress-strain behavior of tubes with $\theta=45^\circ$ and 55° is nonlinear and failure is dominated by matrix cracking and delamination. Recent research utilizing the $\pm 55^\circ$ tubes in construction has also shown the nonlinear stress-strain behavior in tensile coupon tests and CFFTs under bending (Zakaib and Fam 2012; Lu et al. 2020) and in tests utilizing hollow tubes (Betts et al. 2020). Betts et al. (2019) tested 6 hollow $\pm 55^\circ$ GFRP tubes in tension, using two diameter-to-thickness (D/t) ratios of 20 and 45 and reported nonlinear stress-strain responses. The tube with $D/t = 20$ was also filled with concrete and tested in tension by Khan (2020) to evaluate the effects of concrete restraint on the tensile response. Surprisingly, the filled tube obtained a significantly higher tensile strength, 2.1 times that of the hollow counterpart and this was not due to any direct contribution from concrete as it was cracked. A typical FRP lamina displays a nonlinear stress-strain behavior when it is subjected to a transverse tension or in-plane shear (Puck and Mannigel 2007). In $\pm 55^\circ$ and some other angle-ply tubes loaded longitudinally in tension or compression, the above two loading states dominate the global behavior and result in the distinct nonlinear response reported for these tubular members.

The nonlinear tensile response of angle-ply FRP tubes and the remarkably enhanced strength due to concrete filling remain just observations in the very few studies available and are

not fully understood or predictable. In this study, a rigorous finite element (FE) analysis is performed on both hollow tubes and CFFTs to thoroughly understand these phenomena. The calibrated FE model is used in an extensive parametric study, followed by multi-variable regression analysis to develop a simple stress-strain model for angle-ply GFRP tubes in tension. It considers both the inherent nonlinearity and the tensile strength and modulus increase due to concrete filling. The model is intended for accurate strength predictions of CFFTs in flexure, which would otherwise be grossly underestimated using the reported uniaxial properties of the tube.

EXPERIMENTAL DATABASE

To obtain a calibrated, high-fidelity FE model that can be used to develop an accurate stress-strain expression for angle-ply FRP tubes in tension, a robust set of experimental tests was selected for validation purposes, using different test setups, dimensions, and composite properties (Table 1). The first 4 specimens were flat coupons tested in tension, comprising a winding angle (θ) between 30 and 60°, a gross FRP thickness (t) from 2 to 5.4 mm, lengths (L) from 115 to 150 mm, and widths (W) from 12.5 to 25 mm (Table 1). Specimen FE-5 is a small unidirectional (0°) composite plate with two side v-notches prepared and tested according to ASTM D7078 standards (ASTM 2020). With loading applied parallel to the fibers, and due to effects of notching, the specimen is subjected to pure shear stresses at the 45° principal axis direction, resulting in a highly nonlinear behavior.

Specimens FE-6 to FE-9 were all $\pm 55^\circ$ hollow tubes tested in tension by three different researchers (Bai et al. 1997a; Khalifa et al. 2012; Betts et al. 2019). They had a tube diameter (D) of 60-80 mm, L of 300-400 mm, and t of 1.7-5.0 mm. The GFRP tube in specimen FE-10, tested by Khan (2020) and discussed previously, is identical to that in specimen FE-7 but the former was filled with concrete having a compressive strength (f'_c) of 38.5 MPa. The last specimen (FE-11)

is a numerically based one and is added to evaluate the effects of concrete filling for the tube used in specimen FE-6. Specimens FE-10 and FE-11 are identical in every aspect, except t of the tube is 3.8 mm for the former and 1.7 mm for the latter. All tubes in Table 1 were fabricated using E-glass fibers at a fiber volume fraction of 50 to 56%, but contained two resin types, epoxy in specimens FE-1, -2, -3, -4, -5, -8 and vinyl ester in specimens FE-6, -7, -9, -10, -11. The tube's wall (t) consists of a structural part containing the $\pm\theta^\circ$ GFRP layers reported in Table 1 and an epoxy-rich non-structural part, comprising 0.3 mm thick liner as reported by Betts et al. (2019) and Lu et al. (2020).

FINITE ELEMENT MODELING

The FE modeling effort undertaken in this study can be divided into two parts: validation models for the 10 experimental specimens from literature; and a parametric study on 68 additional models of hollow and concrete-filled angle-ply GFRP tubes. The general-purpose commercial software LS-DYNA (2007) was used for the analysis. The authors carried out a previous FE study (Jawdhari et al. 2021) using different constitutive material models and software to aid in the selection of proper modeling methodology for simulating the nonlinear tensile stress-strain behavior of $\pm 55^\circ$ angle-ply GFRP tubes. While LS-DYNA uses an explicit dynamics solver ideal for transient analysis and short duration events, care was taken to ensure a quasi-static simulation by using a relatively large solution time (≥ 2 seconds) coupled with applying the load at a constant velocity of 20 mm/sec to minimize inertial forces. The following sections discuss the model components and details, including element types, mesh, constitutive material relations and loading schemes.

Element Types and Mesh

The GFRP tubes and coupons were modeled by 4-node shell elements, having 6 degrees of

freedom (DOFs) per node and robust stiffness matrix that includes membrane, bending, and shear deformation capabilities (Elsanadedy et al. 2012). The card “Part-Composite” was added to enable stacking of multiple plies, and for each ply, the definition of material, thickness, and orientation. Furthermore, the parameter “LAMSH” was set equal to 1.0 to activate the laminated shell theory for the composite elements and account for through-the-thickness shear strain. The wall of GFRP tube or coupon was assumed to consist of the relevant number of $\pm\theta^\circ$ structural FRP plies sandwiched between two epoxy-rich plies and was modeled as such numerically. It should be noted that when using the shell element, the plies comprising the GFRP tube were assumed to be fully bonded together and thus relative slippage is neglected. The concrete-infill in CFFT specimens and steel plates used for loading and support of both hollow tubes and CFFTs were modeled by 8-node constant stress solid elements. The element, having 3 DOFs per node, utilizes an efficient one-point quadrature reduced integration rule. To minimize the undesirable hourglass modes that are typically present in elements with reduced integration rules, type 4 “hourglass control” was activated for both shell and solid elements (Elsanadedy et al. 2012).

In the single CFFT specimen FE-10 in Table 1, the tube’s inner surface was oiled prior to concrete filling to achieve an ideally frictionless contact between the concrete and GFRP tube. To simulate this condition numerically in this specimen along with FE-11 and all CFFT samples in the parametric study, the contact between the tube and concrete infill was modeled by a surface-to-surface contact, using a cohesion stress of zero and friction coefficient (μ) of 0.2, calibrated and discussed later. Because of the occasional un-symmetric laminate architecture for the angle-ply GFRP composite and to maintain uniformity between all simulations, full-size models were used in validation and parametric study parts, rather than taking advantage of geometric symmetries. The GFRP, concrete, and steel parts were meshed with elements having side lengths of 2 to 8 mm. Boundary conditions imposed in numerical models differed due to various test setups used in Table

1, but in all cases, they mimicked the actual conditions in experimental tests. In general, the boundary conditions consisted of one end being fixed in all directions and the other fixed laterally but allowed to move in the direction of loading.

Material Models

Angle-ply GFRP composite: In this study, MAT 058 “MAT-LAMINATED-COMPOSITE-FABRIC” was selected to model the angle-ply GFRP tubes, following recommendations of several studies (Feraboli et al. 2011; Cherniaev et al. 2018) and milestone applications such as in predicting the impact response of composite members used in Space Shuttle Columbia and CH-46E Sea Knight helicopter (Polanco et al. 2009; Jackson et al. 2017). MAT 058 is a continuum damage mechanics (CDM) based model developed to simulate the nonlinear response, damage initiation, progression and softening for unidirectional laminates and woven fabrics (Zheng 2006). Fig. 1(a) plots a generic stress-strain curve from MAT 058, applicable independently for fiber and matrix directions in either tensile or compressive stress states, as well as for in-plane shear direction. The initial linear response is obtained by defining the elastic and shear moduli and Poisson’s ratios in three orthogonal directions. Similarly, failure initiation can be simulated by defining 5 material strengths: σ_{1t} (tensile in fiber direction), σ_{1c} (compressive in fiber direction), σ_{2t} (tensile in matrix direction), σ_{2c} (compressive in matrix direction) and σ_{12} (in-plane shear). Table 2 lists the key mechanical properties for MAT 058, for three different GFRP lamina utilized in this study.

Three damage variables (ω) are introduced in the compliance matrix relating stress and strain vectors to simulate damage initiation and evolution as follows (Zheng 2006). The variables are applicable for either of the above orthogonal directions.

$$\omega = 1 - e^{-\frac{1}{m} \left(\frac{\varepsilon}{\varepsilon_f} \right)^m} \quad (1)$$

$$m = \frac{1}{\ln\left(\frac{\varepsilon_q}{\varepsilon_f}\right)} \quad (2)$$

where: ε is current strain; ε_f is failure elastic strain (Fig. 1), calculated from dividing the relevant strength by its initial modulus; ε_q is failure strain at which strength is reached (Fig. 1); and m is damage exponent relating ε_q and ε_f . The value of m controls the shape of stress-strain response, where the smaller m is, the more nonlinear and ductile the behavior is and vice versa (Zheng 2006). Further details about the MAT 058 composite model can be found in (Zheng 2006; Polanco et al. 2009; Jackson et al. 2017; Cherniaev et al. 2018).

Fig. 1(b and c) shows the nonlinear stress-strain curves for a typical GFRP lamina under transverse tension and in-plane shear, as obtained from physical tests by Benzarti et al. (2001) and Puck and Mannigel (2007), respectively. These constitutive relations were implemented in MAT 058 model for the three GFRP laminae considered in this study after minor adjustments to their shape, maximum strength, and failure strain to match the properties reported in Table 2. One important aspect is the effect of transverse stress on the shear stress-strain behavior. As can be seen in Fig. 1(c) and reported in Puck and Mannigel (2007), the shear stress-strain response of a unidirectional GFRP lamina softens when a transverse stress is present. This condition is particularly prevalent in angle-ply tubes where the coupling of longitudinal loading and $\pm\theta^\circ$ laminate structure results in an inclined principal axis where both transverse and shear stresses are present. The following stress transformation equations were used for every winding angle (θ) evaluated in the parametric study to calculate the ratio of shear (τ) to transverse (σ_2) stresses for a special loading case under longitudinal stress (σ_x) and adjust shear behavior according to Fig. 1(b).

$$\sigma_2 = \frac{\sigma_x}{2} (1 + \cos 2(\theta + 90)) \quad (3)$$

$$\tau = \frac{\sigma_x}{2} \sin(2 \times \theta) \quad (4)$$

The epoxy-rich layers within the GFRP tube were also modeled by MAT 058, assuming their mechanical properties are identical in each of the orthotropic directions due to isotropy. Table 2 lists the mechanical properties for the epoxy layers, including their elastic and shear moduli and strengths as obtained from (Littell et al. 2008; Betts et al. 2019). Figure 1(d) shows the stress-strain curves under tension, compression and shear as obtained from Littell et al. (2008) for the epoxy-rich layer and used to obtain the correct values for failure strains (ε_q) of the epoxy layer.

Concrete and steel: in specimens FE-10 and FE-11 used for validation purposes, the concrete infill was modeled by material type MAT 159 “MAT-CSCM-CONCRETE”, a plasticity-based model that considers concrete nonlinear characteristics such as cracking and crushing and can be generated from a single parameter, the compressive strength (f'_c) (Elsanadedy et al. 2012). While the model provided good predictions for the specimens and simulated the concrete cracking quite accurately, it resulted in excessive cracking in the models utilized in the parametric study, leading to premature necking and oscillating stress-strain response for the angle-ply GFRP tube. Because the infill is only loaded indirectly with a small axial load through frictional contact with the loaded tube, it remains linear elastic. Also, the exerted radial pressure on the concrete core was well below f'_c . As such, the concrete infill in the parametric study was modeled by an elastic material model “MAT 001”. Elastic modulus (E_c) is the main parameter for material Mat 001 and is defined for concrete based on the American Concrete Institute (ACI 2019) ($E_c = 4700\sqrt{f'_c}$). Typical values of $\nu=0.18$ and $\gamma=2300 \text{ kg/m}^3$ were used for the concrete’s Poisson’s ratio and density, respectively, following recommendations of (Jawdhari and Fam 2018, 2020). Material MAT 001 was also used to model the steel plates, assuming mechanical properties of $E_s= 200 \text{ GPa}$ for elastic modulus, ν and γ of 0.30 and 7850 kg/m^3 , respectively.

VERIFICATION OF MODEL RESULTS

Table 1 reports the maximum stress (σ_{max}) within the tensile stress-strain (σ - ϵ) curves for angle-ply GFRP tubes from testing and numerical models, for the 10 specimens selected from literature to validate the FE model. Apart from specimen FE-6 which will be discussed later, the absolute percentage difference (%Diff.) between numerical and experimental values of σ_{max} ranged between -10.4 and 11.7% with an average of 0.4% for 9 specimens.

Predicted Responses and Failure Modes of Coupons and Hollow Tubes

Figure 2 plots the stress-strain curves from experiments and FE model for the first 4 specimens which were all coupons taken from $\pm\theta^\circ$ GFRP tubes and tested in tension. Besides the good match between the model and test results, the figure shows an interesting nonlinear behavior, particularly for $\theta=45$ and 55° , with the latter resulting in a pseudo elastic-plastic response similar to steel. Figure 3 shows photos of failed specimens alongside the corresponding numerical damage contours at ultimate for representative specimens FE-1, -2, and -5. The failure in the $\pm 55^\circ$ coupons was due to fiber splitting and matrix cracking, while that for the V-notch test (FE-5) was due to shearing and fiber breaking. These failure modes were accurately predicted by the FE model, as can be seen from the similar damage patterns occurring in the numerical samples at ultimate (Fig. 3).

Fig. 4 plots the numerical and experimental σ - ϵ curves for hollow $\pm 55^\circ$ angle-ply tubes under longitudinal tension for specimens FE-6, FE-7 and FE-8. This figure, along with the closely matching failure modes reported in Fig. 5, confirm the model's ability in capturing the tensile behavior of angle-ply hollow tubes. The occasional differences between numerical and experimental responses at ultimate (Table 1 and Fig. 4) can be attributed to minor longitudinal

bending due to misalignment, imperfections in tube thickness or winding angles, and/or the inherent assumptions of the model. A sensitivity analysis is presented later.

Reasons behind Nonlinearity and Failure of Angle-Ply Laminate

To understand the nonlinear behavior and governing mechanisms for $\pm 55^\circ$ FRP tubes, the damage index (DI) along the transverse tension (i.e. normal to the fibers) and shear directions in GFRP plies was extracted from the FE model and plotted in Fig. 6 as a function of loading time (t) for specimens FE-1, and -2. The DI value in fiber direction was very low (i.e. not governing failure), confirming experimental observations that failure of $\pm 55^\circ$ FRP tubes is not governed by fiber rupture (Zakaib and Fam 2012; Lu and Fam 2020). Fig. 6 shows that the DI in transverse tension reaches 1.0 and governs failure, with some effects from in-plane shear damage (DI=0.5-0.55). This explains that the nonlinear response prior to reaching σ_{max} is mainly due to the accumulating matrix cracking under transverse tension. This observation is particularly important given that currently there are no consensus among researchers on whether the failure of angle-ply FRP tubes is caused by the nonlinear matrix shear response or by matrix cracking under transverse tension (Bai et al. 1997a,b ; Zakaib and Fam 2012; Betts et al. 2019).

Predicted Responses and Failure Modes of Concrete-Filled Tube

The axial and circumferential σ - ε responses for $\pm 55^\circ$ angle-ply GFRP tube containing concrete filling (FE-10) is shown in Fig. 7. The FE response matched closely that from testing in both the axial and hoop directions and resulted in a %Diff of only 11% for predictions of σ_{max} . The model was also able to accurately simulate the tube and infill deformations when plotting the infill cracking patterns (Fig. 8(a)) and photos of tube or its model replica at ultimate. Comparing with FE models having μ other than 0.2 which showed material failures (see Fig. 8(b)), the model with

$\mu=0.2$ remained intact throughout the entire analysis. In this model, the tube eventually softened and necking occurred at mid-length due to excessive concrete cracking, but similar to hollow tubes, fibers never failed.

Effect of Concrete Filling on Longitudinal Strength of Tube

Figure 9(a) shows the predicted axial stress versus longitudinal and hoop strain plots of hollow specimens FE-6 and FE-7 with $D/t=45$ and 20, respectively, and their concrete-filled counterparts FE-10 and FE-11. The figure shows that concrete filling has increased σ_{max} of the $\pm 55^\circ$ angle-ply tubes by 2.32 and 3.0 times for the tubes of $D/t=20$ and 45, respectively (Table 1). It also increased stiffness considerably where the behavior is characterized by a bilinear response. Also, CFFT FE-11 with thicker tube showed a 15% higher tensile strength than CFFT FE-10 with thinner tube of the same laminate structure. Figure 9(b) shows the progressive cracking pattern of FE-11 which is associated with load drop events at points 1, 2 and 3 in the stress-strain curve in Fig. 9(a). Because of the concentric axial tension the crack extends across the full cross-section of the core. As such, the remarkable increase in the tube's longitudinal tensile strength in the CFFT system cannot be attributed to any direct longitudinal contribution from the concrete core.

Underlying Phenomenon behind Increased Tube Strength by Concrete Filling

By examining the hoop strains in Fig. 9(a) it can be seen that concrete filling reduces the negative hoop strain of the tube considerably. Therefore, it is hypothesized that a bi-axial tension-tension state of stress develops, including the restrained hoop contraction, which stiffens and strengthens the FRP laminate. To verify this hypothesis, the bi-axial failure envelope of the tube of specimens FE-7 and FE-10 was developed using a small 150x150 mm square plate with the same laminate structure and thickness as the tube. The plate was constrained by hinge-roller supports in each

direction and was subjected to a biaxial tensile loading under different axial-to-hoop stress (σ_x/σ_y) ratios that produce failure. Figure 10 plots the failure envelope for the plate, where the maximum stress in each direction (σ_x, σ_y) is normalized with respect to the uniaxial strength counterparts (σ_{x0} and σ_{y0}). Interestingly, the figure shows that subjecting the $\pm 55^\circ$ GFRP laminate to a biaxial stress state results in a significant increase in laminate strengths in both directions, compared to the uniaxial strengths, which strongly supports the hypothesis. The highest axial strength ratio was 3.0 when the hoop stress ratio was 2.0. Table 3 presents three Damage Indices for each point on the failure envelope, namely fiber tension, matrix tension transverse to fibers and matrix shear parallel to fibers. The table shows that the entire envelope is governed by matrix failure and that fibers fracture does not govern. When hoop tension is predominant, matrix shear failure governs and when axial tension is predominant, matrix tension failure governs.

The axial and hoop stresses of the tube of CFFT specimen FE-10 at every load level are then plotted in Fig. 10, referred to as the ‘loading path’. The intercept of the loading path with the failure envelope indicates failure. At this point, the axial tensile strength ratio (σ_x/σ_{x0}) is 2.29 which is consistent with the increase reported earlier. For reference, the loading path of hollow tube FE-7 is also illustrated in Fig. 10 as a horizontal path along the x-axis reaching stress ratio (σ_x/σ_{x0})=1.0.

Sensitivity Analysis of Key Parameters

Matrix Failure Strain: Figure 11(a and b) plot the (σ - ε) curves for specimen FE-1 from test and FE model with various values for the failure strain (ε_q) in transverse tension and in-plane shear directions, respectively. The figure shows that the response of a $\pm 55^\circ$ angle-ply FRP composite is very sensitive to the lamina’s stress-strain curves in transverse tension and shear and their corresponding failure strains. Therefore, the results of this study and the design model should only be used within the context of the laminate properties in Table 2 which are fabricated using E-glass

fibers embedded in epoxy or vinyl ester resins, at fiber volume fraction of 50-56%.

Fiber Winding Angle: Figure 11(c), shows the numerical σ - ε curves for specimen FE-6 with $\theta = 55, 57.5$ and 60° . The tube's response is seen to be sensitive to θ , where varying the angle from a nominal value of 55° to a slightly larger 60° angle (only 9%), resulted in changing the percentage of numerical-to-experimental difference in σ_{max} from 30 to 15% (i.e. a 50% difference). In addition to effects of θ and other factors related to the physical experiment such as unintended load misalignment or curvature, limitations on the FE model part such as mesh size effects and approximations of material properties, can also cause deviations of predictions from testing results.

Friction Coefficient: Figure 11(d), shows the calibration process of the friction coefficient (μ) for a range of zero to 0.3. Although the tube was initially lubricated prior to concrete casting, some residual frictional forces are expected to develop at the interface. The figure shows that a $\mu=0.2$ can reasonably simulate the interface and results in σ_{max} comparable to experimental value.

Loading Speed: Figure 11(e and f) show the effect of loading speed (v) on the behavior of hollow tube (FE-7) and its CFFT counterpart (FE-10). It was found that varying v from 10 to 30 mm/s has negligible effects on the response and thus a value of 20 mm/s was used in the subsequent parametric study.

PARAMETRIC STUDY

Three key variables were studied in this section, namely: (D/t) ratio from 25 to 100, winding angle (θ) from 35 to 75° , and (f'_c) from 20 to 80 MPa. The last parameter is fully studied using four f'_c values for $\theta=55^\circ$ while for other angles, only two values, $f'_c=20$ and 60 MPa were evaluated. A tube with a gage length (L) of 500 mm, a diameter (D) of 100 mm, and lamina's properties identical to those given in Betts et al. (2019) for specimens FE-6, -7, and -10 (Table 1) was used for all parametric study models. It should be noted when varying D/t ratio, a symmetric distribution of \pm

θ° layers was maintained for each selected (t) value, resulting in a slightly different actual D/t ratio for a few specimens than the nominal ones reported in Tables 3 and 4. All other geometrical and mechanical properties as well as modeling strategies for the parametric study are the same as those used in the validation analysis discussed previously. Tables 4 and 5 list the 68 new models, including 20 for hollow tubes and 48 for CFFTs, their properties and key results.

Hollow Angle-Ply GFRP Tubes

Table 4 lists σ_{max} , axial tensile strain at σ_{max} (ε_{x-max}), and hoop strain at σ_{max} (ε_{y-max}) for the 20 hollow angle-ply GFRP tubes with different D/t ratios and θ values. The σ - ε responses for these tubes along with their CFFT counterparts are graphically presented in Fig. 12 for selected samples. It can be seen from the results that increasing D/t ratio from 25 to 100 for $\theta=65$ and 75° results in a negligible reduction in σ_{max} , but for $\theta=35, 45$ and 55° causes a 5-12% decrease in σ_{max} . For all D/t ratios, increasing θ results in decreasing σ_{max} significantly, where for example varying θ from 35 to 75° at $D/t=25$ causes an 80% reduction in σ_{max} . On the other hand, ε_{x-max} and ε_{y-max} are negligibly affected by D/t ratio but generally decrease with θ (Fig. 12). Failure modes in these hollow tubes was due to stability, either by necking at central or end sections, or localized buckling (Table 3 and Fig. 13). The σ - ε curves shown in Fig. 12 for $\theta=35, 45$ and 55° show a typical nonlinear response in both axial and hoop directions, confirming earlier results and discussions about the interesting behavior of angle-ply FRP tubes. Deformed shapes of the hollow tubes can be seen in Fig. 13 (a to c).

Concrete-Filled Angle-Ply GFRP Tubes

Table 5 lists the developed CFFT models with different D/t ratios, θ and f'_c values, and key analysis results. Comparing σ_{max} of hollow tubes in Table 4 with that of the CFFT counterparts in Table 5

and their respective σ - ε curves in Fig. 12, the effects of concrete filling on tensile stress-strain response and ultimate strength of angle-ply FRP tubes become staggeringly clear. Material failure of the tube occurred in all cases as seen in Fig. 13(d). Concrete filling resulted in a much stiffer σ - ε response and higher σ_{max} for all D/t and θ values. This trend can further be seen in Fig. 14 when plotting the stress enhancement ratio (α) which is the ratio between σ_{max} of a CFFT to that of the hollow tube, against D/t ratio for $f'_c=20$ and 60 MPa, and all θ values. In general, α ranged between 1.30 to 4.46, with an average of 2.91, 4.11, 3.29, 2.77, and 1.43 for $\theta=35, 45, 55, 65$ and 75° respectively, across all D/t and f'_c values. Fig. 15 shows that f'_c has an insignificant effect on σ_{max} and α .

PROPOSED DESIGN-ORIENTED EQUATION

To implement the accurate nonlinear stress-strain behavior of angle-ply tubes filled with concrete into analytical procedures such as flexural strength calculation of CFFTs, a design-oriented equation in the form of a single mathematical formula is proposed in this section. Experimental and numerical results presented so far suggest that the longitudinal stress-strain curves are almost bilinear with two distinctive initial and secondary slopes connected with a nonlinear transition zone. To model this bilinear behavior, the Richard-Abbott (1975) equation was adopted as follows:

$$f(\varepsilon) = \frac{(E_1 - E_2) \cdot \varepsilon}{\left[1 + \left(\frac{E_1 - E_2}{f_u - E_2 \varepsilon_u}\right)^n\right]^{1/n}} + E_2 \cdot \varepsilon \quad (5)$$

where f is the longitudinal stress, ε is the longitudinal strain, E_1 is the initial modulus, and E_2 is the secondary modulus, f_u is the peak stress ($=\sigma_{max}$ in previous sections), ε_u is the peak strain, and n is the shape parameter defining the degree of curvature of the transition zone as shown in Fig. 16(a). The mathematical expression has also been adopted for modeling the behavior of FRP-confined concrete (Pantelides and Yan 2007; Wu and Wei 2015; Khorramian and Sadeghian 2021) in the

past. However, this is the first time to implement it for modeling the nonlinearity of FRP in the context of angle-ply CFFTs in tension. The parameters of the equation can be calibrated for any bilinear behavior.

In this study, a regression analysis on critical parameters of the stress-strain curves, namely f_u , ε_u , E_1 , and E_2 was performed. The parameters were obtained based on the parametric study (see Table 5). As previously demonstrated, the FRP response was only sensitive to the fiber orientation (θ) of the FRP tube and was not much affected by f'_c or D/t ratio. Figure 17 shows the variation of key parameters of Eq. 5 with θ . Overall, as θ changed from 35 to 75 degrees, the peak stress and strain showed a logarithmic (Eq. 6) and linear (Eq. 7) relationship with θ , respectively (Fig. 17a and 17b). Also, the initial modulus showed a quadratic relationship (Eq. 8) with θ (Fig. 17c). The ratio of the secondary modulus to the initial modulus (E_2/E_1) showed a linear relationship (Eq. 9) with θ (Fig. 17d).

$$f_u = 2658 - 604Ln(\theta) \quad (6)$$

$$\varepsilon_u = 0.0227 + 0.0002\theta \quad (7)$$

$$E_1 = 45000 - 841\theta + 4.71\theta^2 \quad (8)$$

$$E_2/E_1 = 1.36 - 0.017\theta \quad (9)$$

In these equations, the angle θ is in degree, the stress and moduli are in MPa, and the strain is in mm/mm. The shape parameter (n) was calibrated to 2.5 based on comparing the performance of the proposed equation and FEM results ($f'_c=20$ MPa, and $D/t= 75$) as shown in Fig. 16(b). The figure indicates that the proposed design-oriented equation has a very good agreement with the FEM results.

CONCLUSIONS

In this study, the longitudinal tensile behavior of angle-ply fiber-reinforced polymer (FRP) tubes

is studied and compared for hollow and concrete-filled FRP tubes (CFFTs) using a nonlinear finite element (FE) model developed in LS DYNA software. The model successfully predicted the nonlinearity of angle-ply coupons and hollow tubes as well as the bi-linear response of tubes in CFFTs from a diverse experimental database compiled from literature. A parametric study was also performed to examine the effects of major parameters including diameter-to-thickness (D/t) ratio, fiber angle from longitudinal axis (θ), and concrete compressive strength (f'_c) for CFFT members. The following conclusion can be drawn from this study:

1. The behavior of angle-ply FRP tubes (e.g. $\pm 55^\circ$) under longitudinal tension is completely different whether they are hollow or concrete-filled, with the latter experiencing significantly increased tensile strength and stiffness. This is because the concrete core fundamentally changes the composite laminate behavior as demonstrated by the model, and is not attributed to any direct longitudinal contribution from concrete which is cracked.
2. Concrete filling restrains the large radial and circumferential contraction that occur in hollow tubes, thereby generates significant hoop tensile stresses. Together with the primary longitudinal tension, this places the tube in a state of bi-axial tensile stress. The failure envelope under such stress combination far exceeds the uniaxial strength in either direction. For example the longitudinal tensile strength (σ_{max}) of a $\pm 55^\circ$ tube increased by 2.3 and 3.0 times for $D/t=20$ and 45, respectively.
3. The parametric study showed that the average ratio (α) between σ_{max} of a CFFT tube and that of the hollow counterpart is highly dependent on angle θ . For $\theta=35, 45, 55, 65$ and 75° , α was 2.9, 4.1, 3.3, 2.8, and 1.4, respectively. Concrete strength has an insignificant effect on α .
4. The parametric study showed that for hollow tubes, increasing D/t from 25 to 100 results in a negligible reduction in longitudinal tensile strength (σ_{max}) for $\theta=65-75^\circ$, but for $\theta=35-$

- 55° it causes a 5-12% decrease in σ_{max} .
5. For all D/t ratios, increasing θ in hollow tubes results in decreasing σ_{max} significantly, where for example varying θ from 35 to 75° at $D/t = 25$ causes an 80% reduction in σ_{max} .
 6. Design-oriented equations have been developed to represent the longitudinal bi-linear stress-strain curve of angle-ply tubes when filled with concrete as a function of the single most influencing parameter, θ . This can be implemented in sectional analysis of flexural strength of CFFTs which would otherwise be grossly underestimated when using the reported tensile strength of hollow tube.

DATA AVAILABILITY STATEMENT

All data, models, and code generated or used during the study appear in the published article

ACKNOWLEDGMENTS

The authors wish to acknowledge the financial support provided by the MITACS Elevate program and NSERC Discovery grant program.

REFERENCES

ACI. Building Code Requirements for Structural Concrete (ACI 318-19) and Commentary on Building Code Requirements for Structural Concrete. American Concrete Institute Farmington Hills, MI 2019.

Ashraf, M.A., Morozov, E.V., Shankar, K. 2014. "Flexure analysis of spoolable reinforced thermoplastic pipes for offshore oil and gas applications." J. Reinforc. Plast. Compos. 33, 533–

ASTM D7078, (2020). “Standard Test Method for Shear Properties of Composite Materials by V-Notched Rail Shear Method,” ASTM International, 100 Barr Harbor Drive, PO Box C700, West Conshohocken, PA 19428-2959.

Bai, J. B., Hu, G. K. and Bompard, Ph. 1997b. “Mechanical behavior of $\pm 55^\circ$ filament-wound glass-fibre/epoxy resin tubes: Part II—Micromechanical modelling of the damage initiation-competition of the different mechanisms.” *Compos. Sci. Technol.*, 1997, 57, 155–164.

Bai, J. B., Seeleuthner, Ph. and Bompard, Ph. 1997a. “Mechanical behavior of $\pm 55^\circ$ filament-wound glass-fibre/epoxy resin tubes: Part I—Microstructure analyses and mechanical behavior and damage mechanisms of composite tubes under pure tensile, pure internal pressure and combined loading.” *Compos. Sci. Technol.*, 57, 141–153.

Benzarti K, Cangemi L, Dal Maso FD. 2001. “Transverse properties of unidirectional glass/epoxy composites: influence of fibre surface treatments.” *Compos Part A Appl Sci Manuf*, 32, pp. 197–206. [https://doi.org/10.1016/S1359-835X\(00\)00136-6](https://doi.org/10.1016/S1359-835X(00)00136-6).

Betts, D., Sadeghian, P., and Fam, A. 2019. “Investigation of the stress-strain constitutive behavior of $\pm 55^\circ$ filament wound GFRP pipes in compression and tension”, *Composites Part B: Engineering*, 172, pp. 243-252.

Betts, D., Sadeghian, P., and Fam, A. 2020. “Experimental and analytical investigations of the flexural behavior of hollow $\pm 55^\circ$ filament wound GFRP tubes.” *Thin-Walled Structures*, 159, 107246. <https://doi.org/10.1016/j.tws.2020.107246>

Carroll, M., Ellyin, F., Kujawski, D., Chiu, A. S. 1995. “The rate-dependent behaviour of $\pm 55^\circ$ filament-wound glass-fibre/epoxy tubes under biaxial loading”, *Compos. Sci. Technol.* 55, 391–403

Chenxi Lu, Fam, A. 2020. “The effect of tube damage on flexural strength of $\pm 55^\circ$ angle-ply concrete-filled FRP tubes.” *Construction and Building Materials*. 240, 117948, ISSN 0950-0618, <https://doi.org/10.1016/j.conbuildmat.2019.117948>.

Cherniaev, A. Montesano, J. Butcher, C. 2018. “Modeling the axial crush response of CFRP tubes using MAT054, MAT058 and MAT262 in LS-DYNA.” In Proceedings of the 15th International LS-DYNA Users Conference, 10–12 June, Detroit, MI, USA, pp. 1–17.

Elsanadedy, H. M., Al-Salloum, Y. A., Alsayed, S. H., Iqbal, R.A. 2012. “Experimental and numerical investigation of size effects in FRP-wrapped concrete columns.” *Construction and Building Materials*, 29, 56-72.

Fam, A., Pando, M., Filz, G., Rizkalla, S. 2003b. “Precast piles for route 40 bridge in Virginia using concrete filled FRP tubes.” *PCI J.* 48–3, 32–45.

Fam, A., R. Greene, and S. Rizkalla. 2003a. “Field applications of concrete filled FRP tubes for marine piles.” *ACI Spec. Publ.* 48 (3): 161–180.

Feraboli, P., Wade, B., Deleo, F., Rassaian, M., Higgins, M., Byar, A. 2011. “LS-DYNA MAT54 modeling of the axial crushing of a composite tape sinusoidal specimen.” *Composites Part A: Applied Science and Manufacturing*, 42 (11), pp. 1809-1825.

Hollaway, L.C.M.B. Leeming, *Strengthening of Reinforced Concrete Structures using Externally Bonded FRP Composites in Structural and Civil Engineering*. 2000, Boca Raton, FL, USA: CRC Press LLC.

Ibrahim S, Polyzois D, Hassan S. 2000. “Development of glass fiber reinforced plastic poles for transmission and distribution lines.” *Canadian Journal of Civil Engineering*;27(5):850–8.

Jackson KE, Fasanella EL and Littell JD. 2017. “Development of a continuum damage mechanics material model of a graphite-Kevlar hybrid fabric for simulating the impact response of energy absorbing subfloor concepts.” Fort Worth, TX, USA, 2017, <https://ntrs.nasa.gov/search.jsp?R=20170005463> () p. 12.

Jawdhari, A., Adheem, A., and Kadhim, M. 2020. “Parametric 3D Finite Element Analysis of FRCM-Confined RC Columns under Eccentric Loading.” *Engineering Structures*, vol 212.

Jawdhari, A., and Fam, A. 2018. “Numerical Study on Mechanical and Adhesive Splices for Ribbed GFRP Plates Used in Concrete Beams.” *Engineering Structures*, vol 174, p478-494.

Jawdhari, A., and Fam, A. 2020. “A New Studded Precast Concrete Sandwich Wall with Embedded GFRP Channel Sections - Part II: Finite Element and Parametric Studies.” *PCI Journal*, vol 65(4), pp. 51-70.

Jawdhari, A., Fam, A., Sadeghian, P. 2021. “Modeling the Nonlinear Response of $\pm 55^\circ$ Angle-Ply GFRP Tube used in CFFT Applications.” Submitted to 8th international conference on advanced composite materials in bridges and structures, 18-20 August, Sherbrooke, Quebec, Canada.

Khalifa, A. B., Zidi, M., Abdelwahed, L. (2012). “Mechanical characterization of glass/vinylester $\pm 55^\circ$ filament wound pipes by acoustic emission under axial monotonic loading.” *Comptes Rendus Mecanique*, 340, pp. 453–460.

Khan, S. 2020. “Structural properties of commercially used $\pm 55^\circ$ filament wound GFRP pipes filled with concrete in tension.” Technical Co-op Report submitted to the Department of Civil and Resource Engineering, Dalhousie University, Halifax, NS, Canada.

Khorramian, K., and Sadeghian P. (2021). “New mechanics-based confinement model and stress-strain relationship for analysis and design of concrete columns wrapped with FRP composites.” *Structures Journal*. (under review).

Littell, J. D., Ruggeri, C. R., Goldberg, R. K., Roberts, G. D., Arnold, W. A., and Binienda, W. K. 2008. “Measurement of epoxy resin tension, compression, shear stress-strain curves over a wide range of strain rates and temperatures.” *J. Aerosp. Eng.*, 21 (3), pp. 162–173.

LS-DYNA User’s Keyword Manual, vol. 1. Version 971. Livermore Software Technology Corporation (LSTC); 2007.

Lu, C., St. Onge, J., Fam, A. 2020. “Damage threshold of near-cross-ply tubes used in concrete-filled FRP tubes loaded in flexure.” *J. Compos. Constr.* 24 (2),

[https://doi.org/10.1061/\(ASCE\)CC.1943-5614.0000990](https://doi.org/10.1061/(ASCE)CC.1943-5614.0000990).

- Mandal, S. and Fam, A. 2006. "Modeling of Prestressed Concrete-Filled Circular Composite Tubes Subjected to Bending and Axial Loads." *ASCE Journal of Structural Engineering*, 132(3):449-459.
- Mitchell, J., Fam, A. 2010. "Tests and analysis of cantilevered GFRP tubular Poles with partial concrete filling." *J. Compos. Construct.* 14 (2010) 115–124.
- Olivares, G., Acosta, J.F., Yadav, V., Keshavarayana, S., and Abramowitz, A. "Crashworthiness of Composites Structures – Coupon Level Material Model Development." FAA JAMS 2011 Technical Review Meeting, April, 2011.
- Pantelides, C. P., and Yan, Z. (2007). Confinement model of concrete with externally bonded FRP jackets or posttensioned FRP shells. *Journal of Structural Engineering*, 133(9), 1288-1296.
- Parnas, L., Katirci, N. 2002. "Design of Fiber-Reinforced Composite Pressure Vessels Under Various Loading Conditions." *Composite Structures*, 58, 83-95.
- Polanco M. A., Kellas S., and Jackson K. E. 2009 "Evaluation of Material Models within LS-DYNA for a Kevlar®/Epoxy Composite Honeycomb." *Proceedings of the 65th AHS Forum*, Grapevine, TX, May 27-29.
- Puck A, Mannigel M. 2007. "Physically based non-linear stress-strain relations for the inter-fibre fracture analysis of FRP laminates." *Compos Sci Technol*;67, pp 1955–1964.
<https://doi.org/10.1016/j.compscitech.2006.10.008>.
- Rafiee, R. 2016. "On the mechanical performance of glass-fibre-reinforced thermosetting resin pipes: a review." *Compos. Struct.* 143, 151–164.
- Richard, R. M., and Abbott, B. J. (1975). Versatile elastic-plastic stress-strain formula. *Journal of the Engineering Mechanics Division*, 101(4), 511-515.
- Shao, Y., Mirmiran, A. 2005. "Experimental investigation of cyclic behavior of concrete filled fiber reinforced polymer tubes." *J. Compos. Construct.* 9 (2005) 263–273.

Sodden, P. D., Kitching, R., Tse, P. C., and Tsavalas. Y. 1993. "Influence of winding angle on the strength and deformation of filament-wound composite tubes subjected to uniaxial and biaxial loads." *J Compos Science& Tech*, 46, pp. 363–378.

Son JK, Fam A. 2008. "Finite element modeling of hollow and concrete-filled fiber composite tubes in flexure: model development, verification and investigation of tube parameters." *Engineering Structures*; 30(10):2656–66.

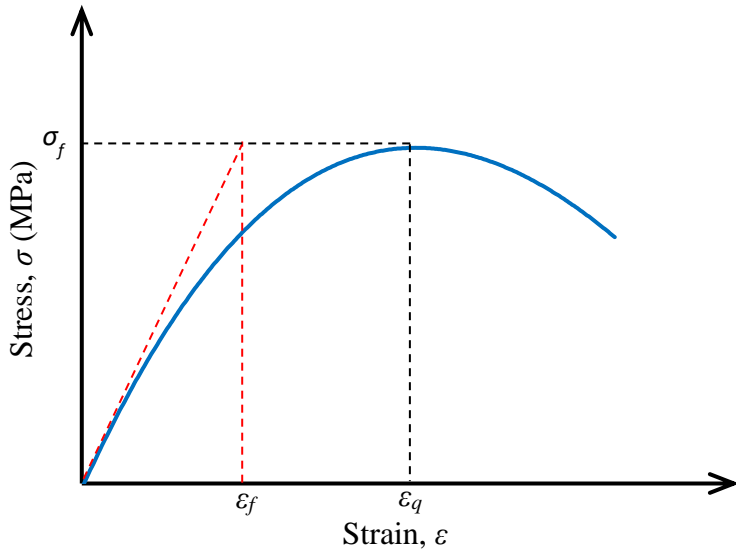
Tomblin, J., McKenna, J., Ng, Y., and Raju, K. S. 2001. "B-Basis Design Allowables for Epoxy – Based Prepreg Newport E-Glass Fabric 7781/NB321." *Advanced General Aviation Transport Experiments (AGATE)-WP3.3-033051-097*.

Wu, Y. F., and Wei, Y. (2015). General stress-strain model for steel-and FRP-confined concrete. *Journal of composites for construction*, 19(4), 04014069.

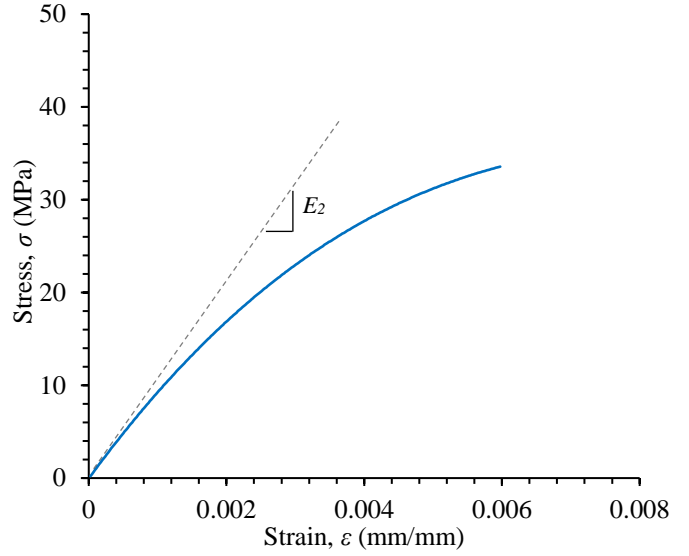
Xie, P., Guan Lin, Teng, J.G., Jiang, T. 2020. "Modelling of concrete-filled filament-wound FRP confining tubes considering nonlinear biaxial tube behavior.", *Engineering Structures*. 218,110762, ISSN 0141-0296, <https://doi.org/10.1016/j.engstruct.2020.110762>.

Zakaib, S., and Fam, A. 2012. "Flexural performance and moment connection of concrete concrete-filled GFRP tube-encased steel I-sections." *J Compos Constr ASCE* 16(5), pp. 604–613.

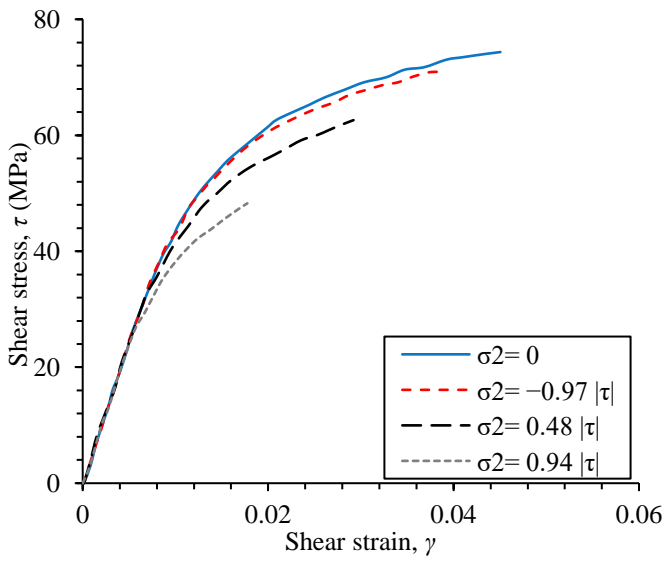
Zheng, X. 2006. "Nonlinear strain rate dependent composite model for explicit finite element analysis." PhD dissertation, University of Akron, Ohio, USA.



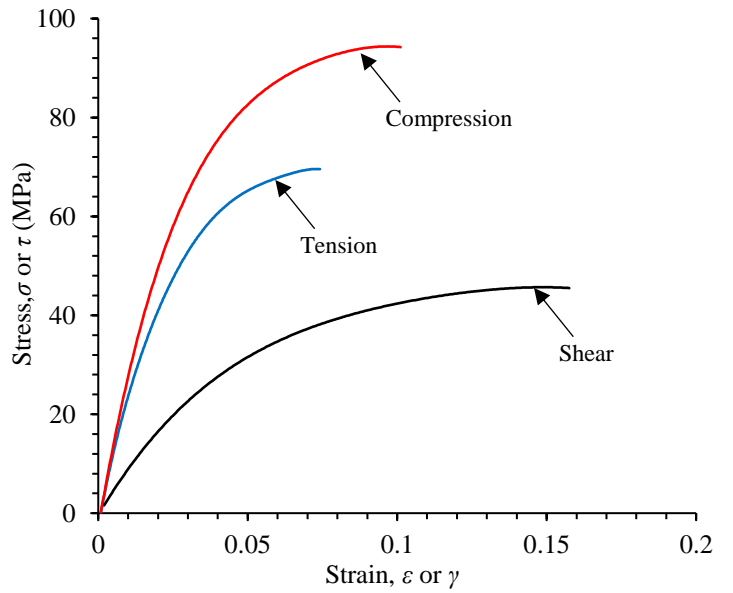
(a)



(b)



(c)



(d)

Figure 1. Constituent stress-strain relations used in current study, (a) typical stress-strain curve implemented for MAT 058 in LS DYNA software, (b) and (c) GFRP lamina under transverse tension and in-plane shear, respectively, and (d) epoxy-rich layer.

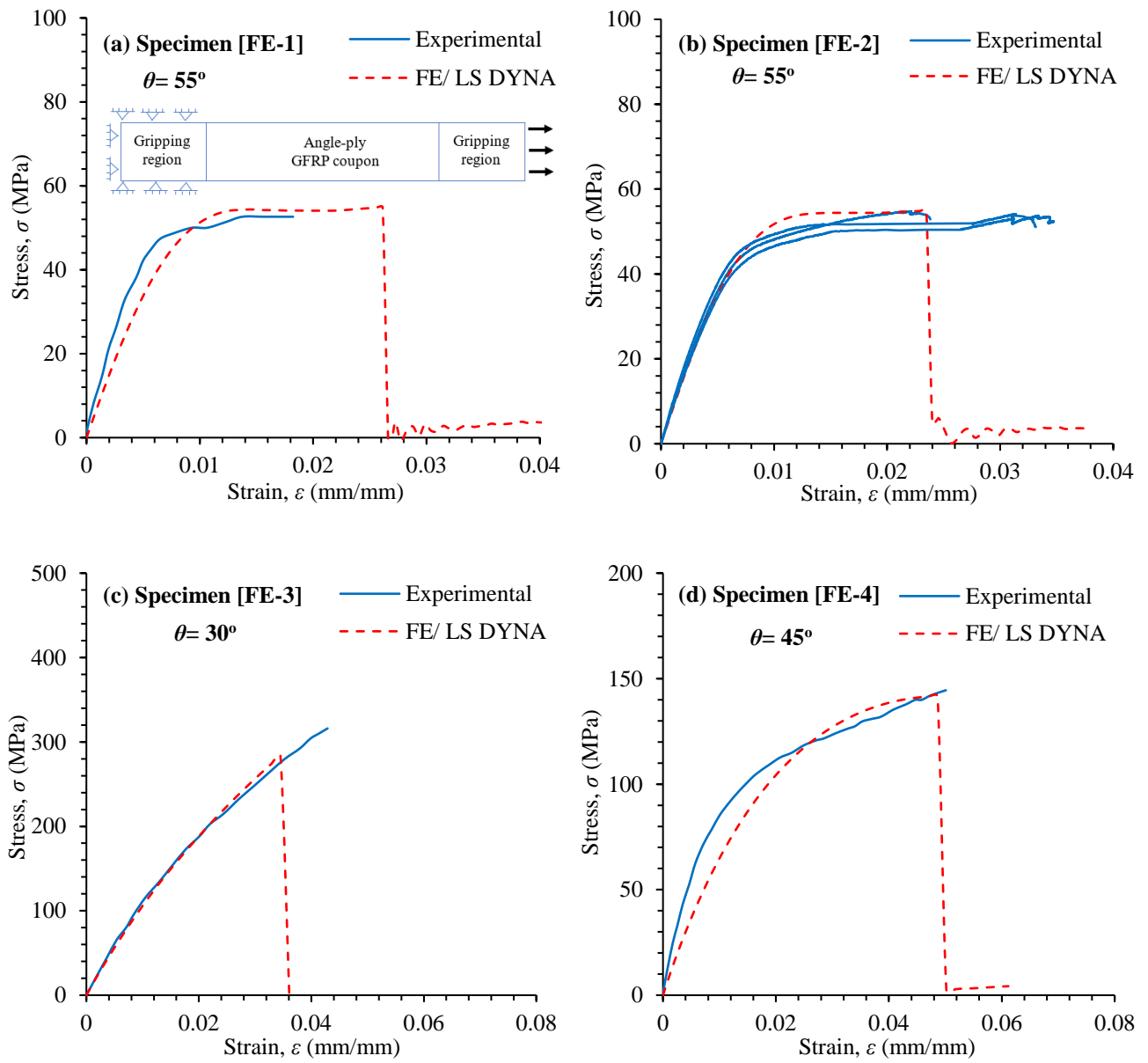
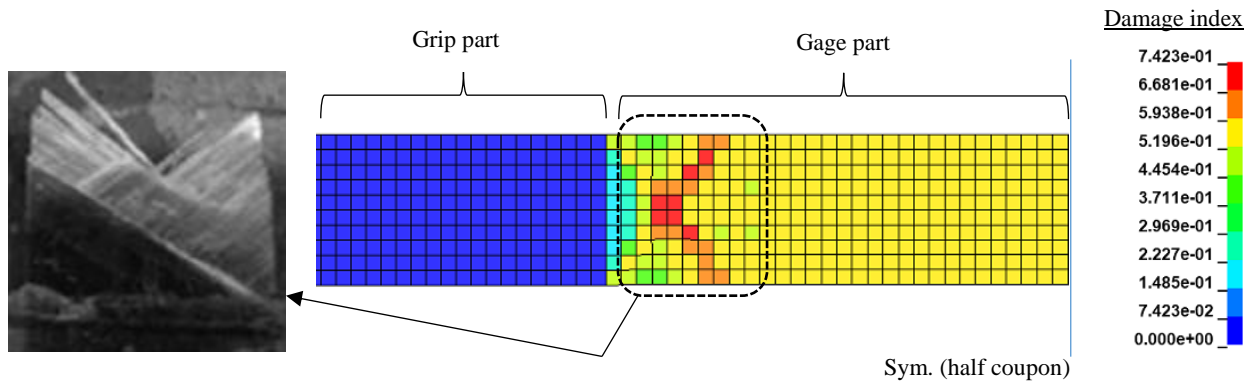
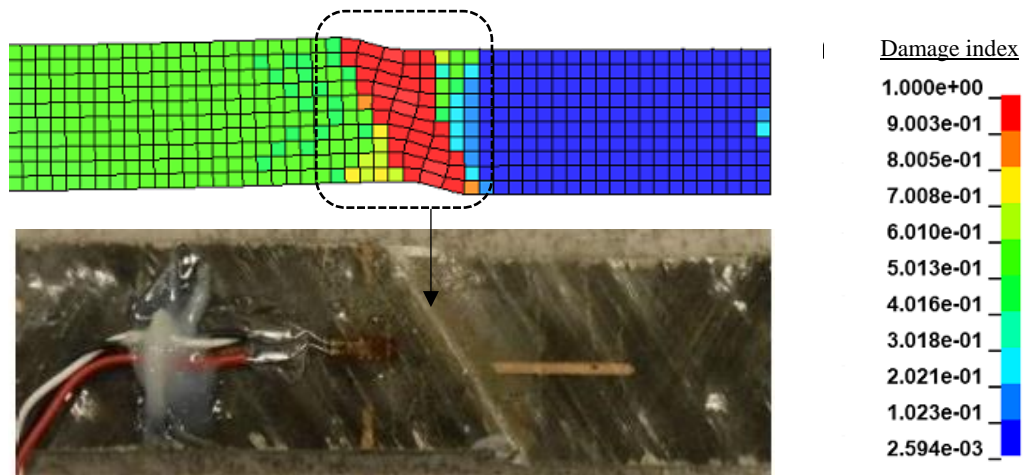


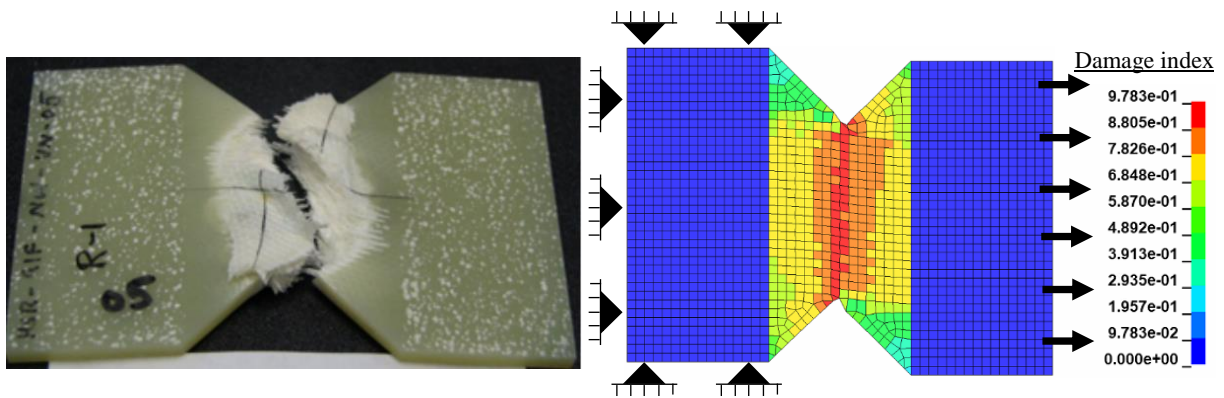
Figure 2. Test and FE predicted axial stress-strain curves, $\pm\theta^\circ$ GFRP coupon specimens.



(a) Specimen FE-1 (flat coupon).



(b) Specimen FE-2 (flat coupon).



(c) Specimen FE-5 (V-notch shear).

Note: damage index ranges from 0 (undamaged) to 1.0 (fully damaged).

Figure 3. FE simulation of failure modes in angle-ply FRP tensile specimens.

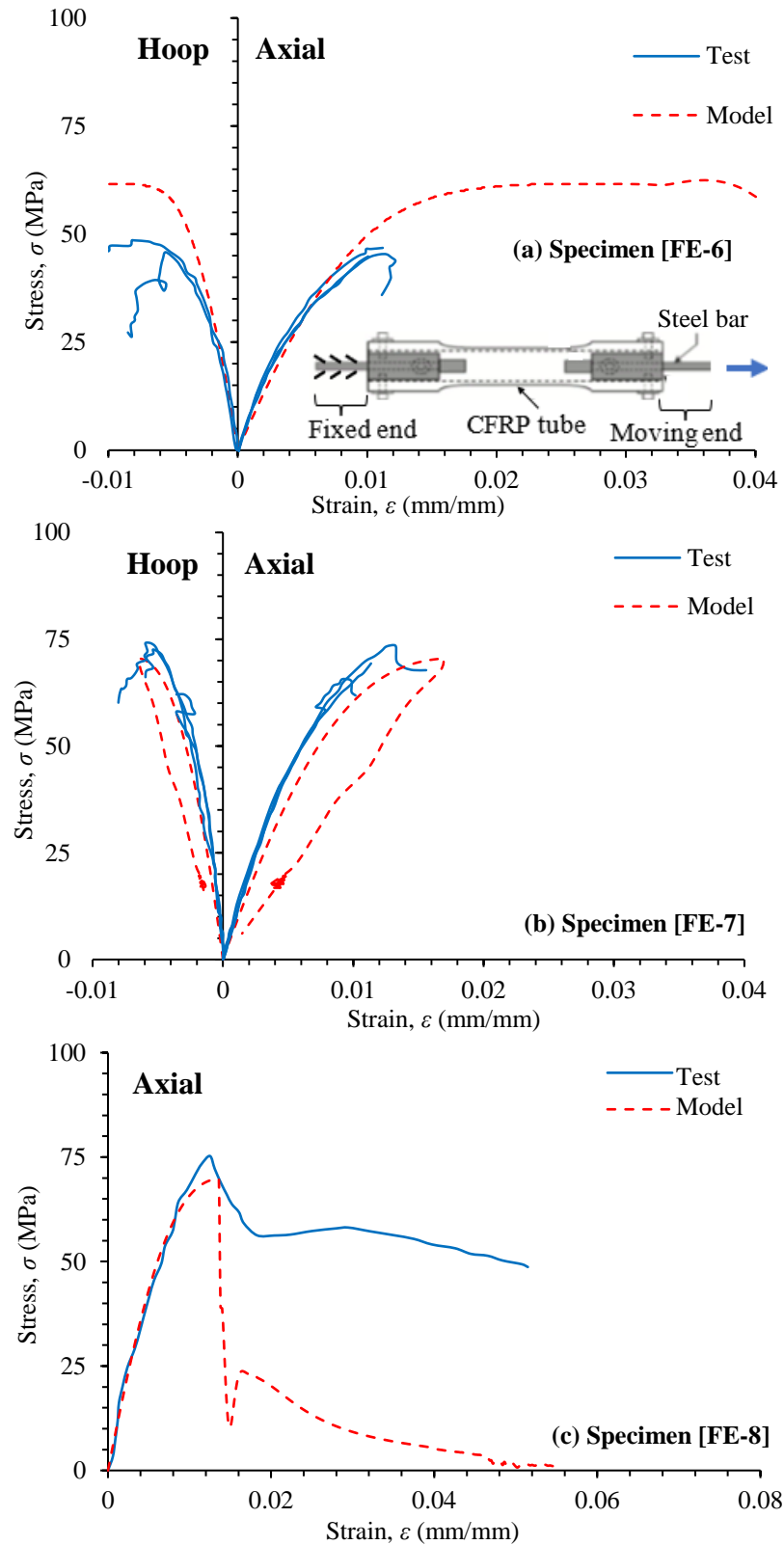
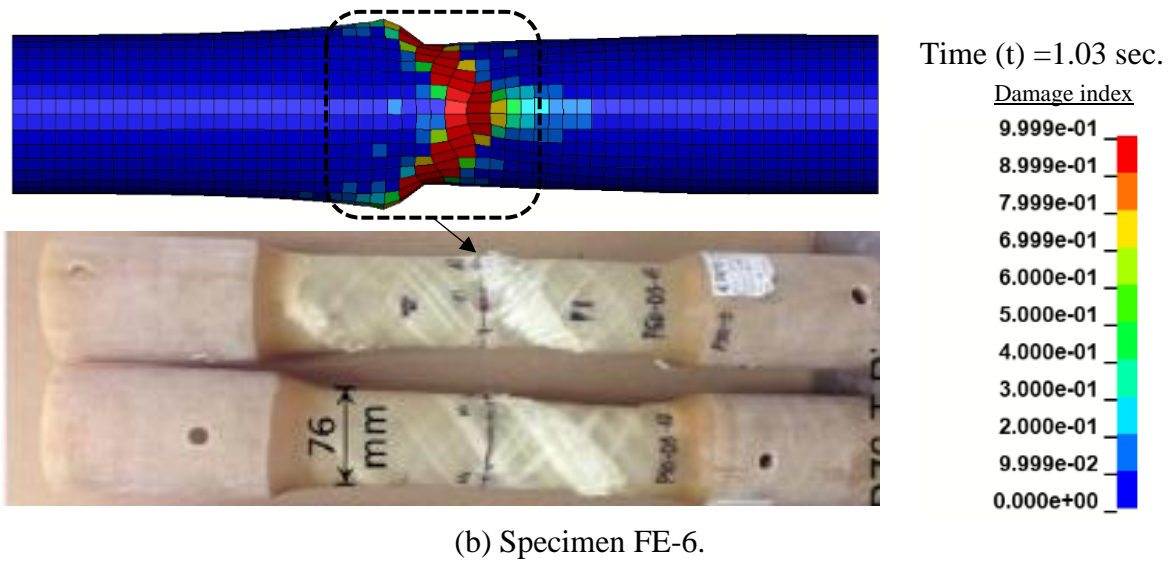
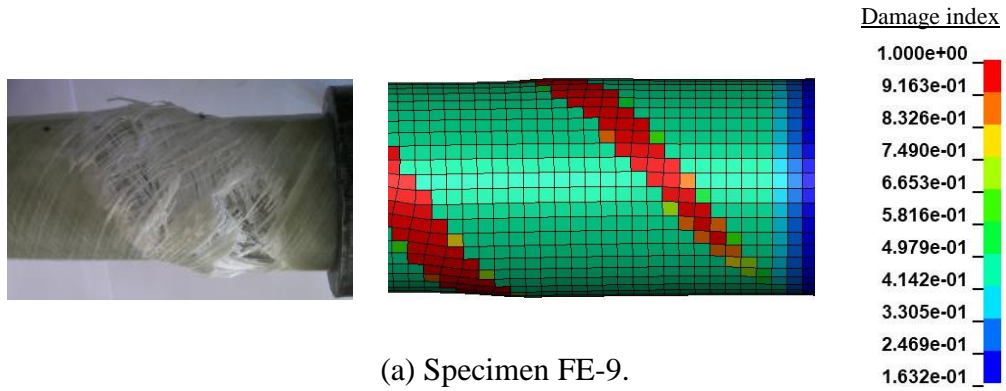
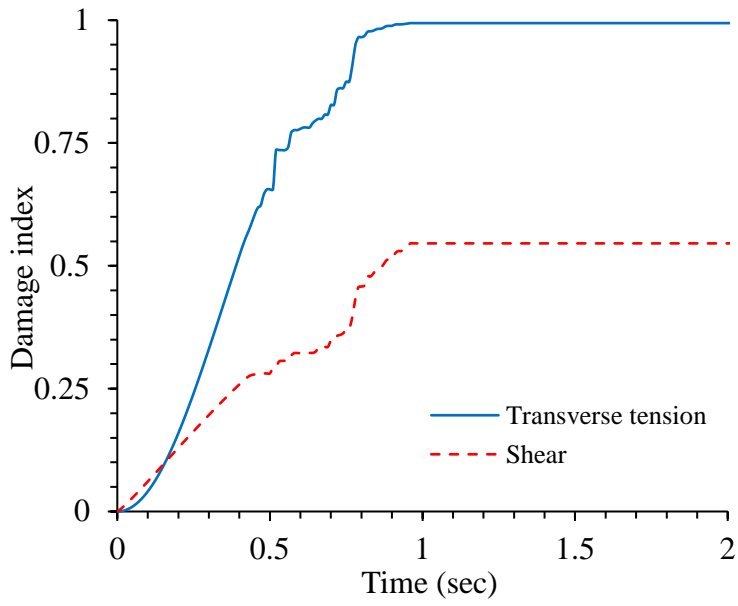


Figure 4. Test and FE predicted stress-strain curves, $\pm 55^\circ$ GFRP hollow tube specimens.

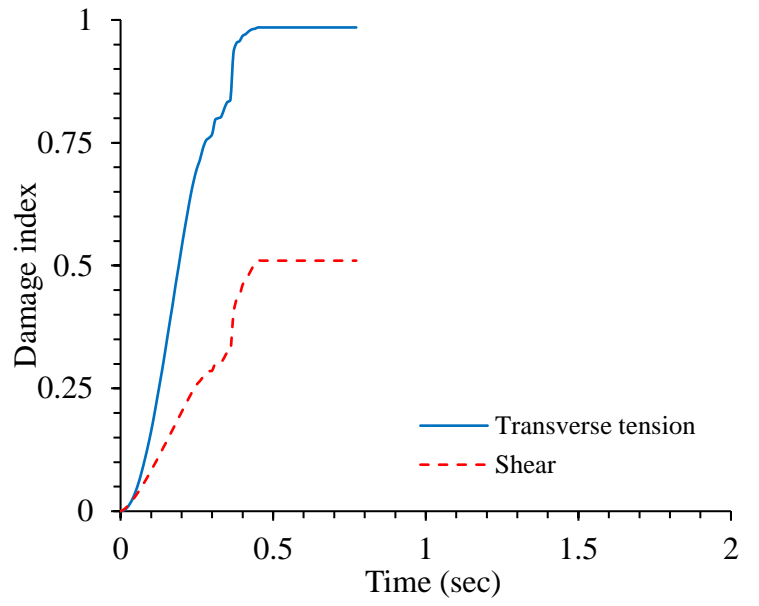


Note: damage index ranges from 0 (undamaged) to 1.0 (fully damaged).

Figure 5. FE simulation of failure modes in $\pm 55^\circ$ GFRP hollow tube specimens.



(a) Specimen FE-1



(b) Specimen FE-2

Figure 6. Damage index vs. time curves, for transvers tension and shear modes in FRP lamina.

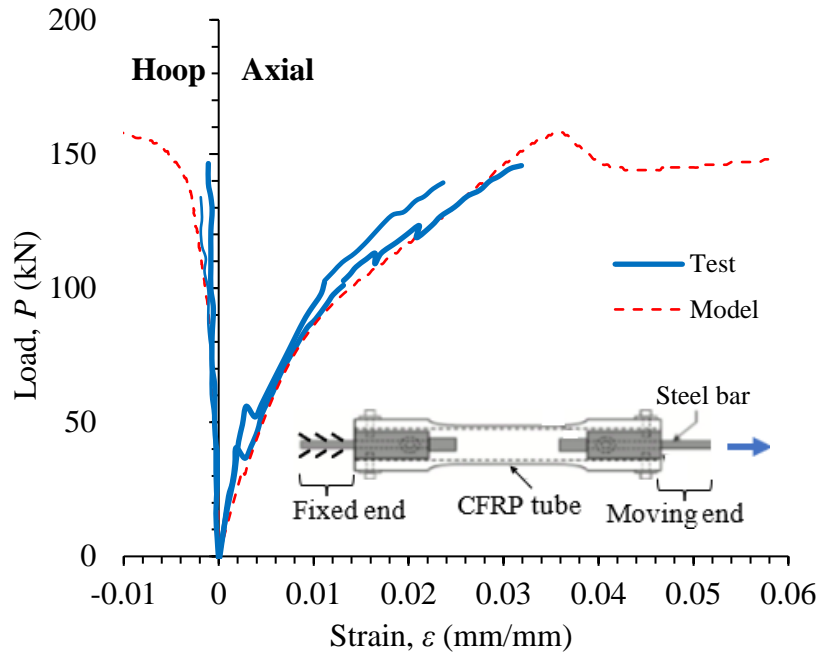
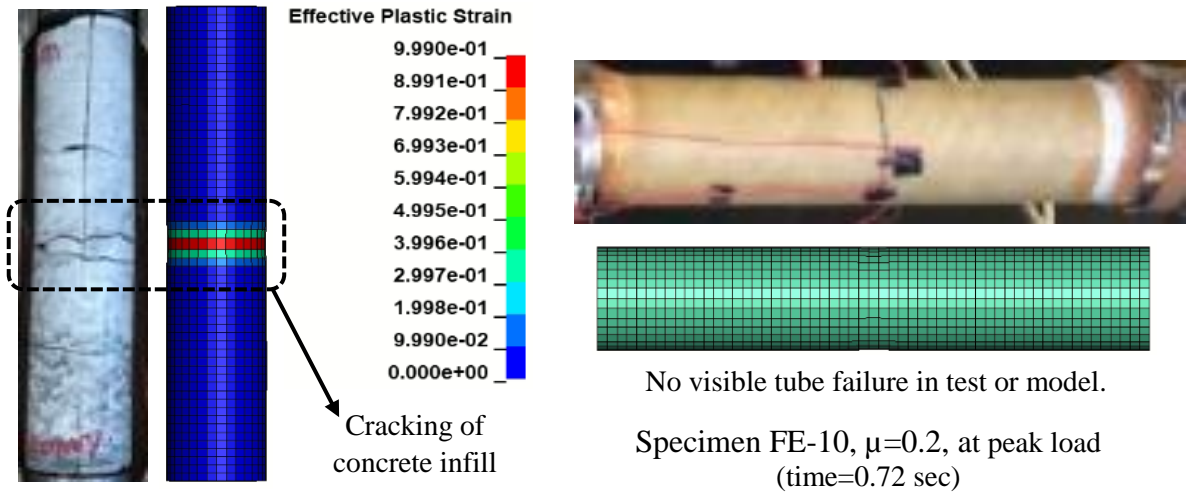
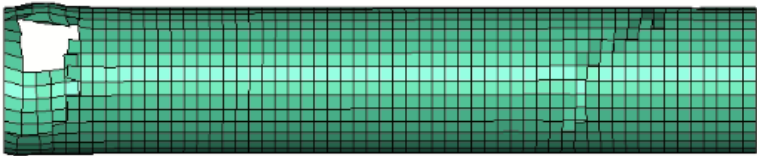
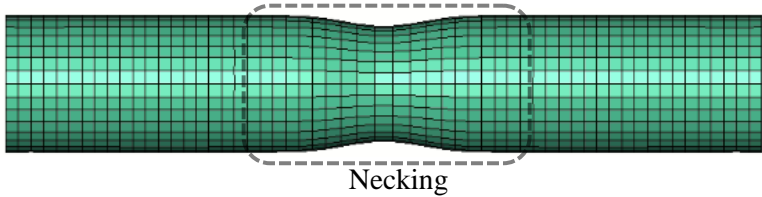
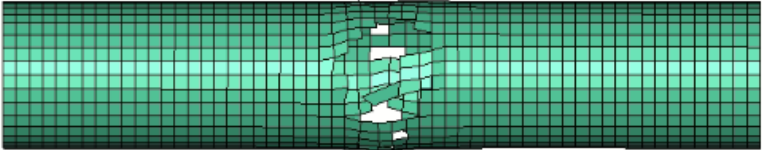
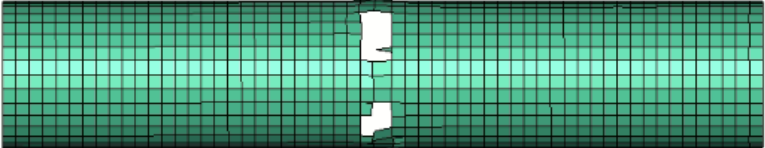


Figure 7. Test and FE predicted stress-strain curves, $\pm 55^\circ$ GFRP CFFT specimen (FE-10)



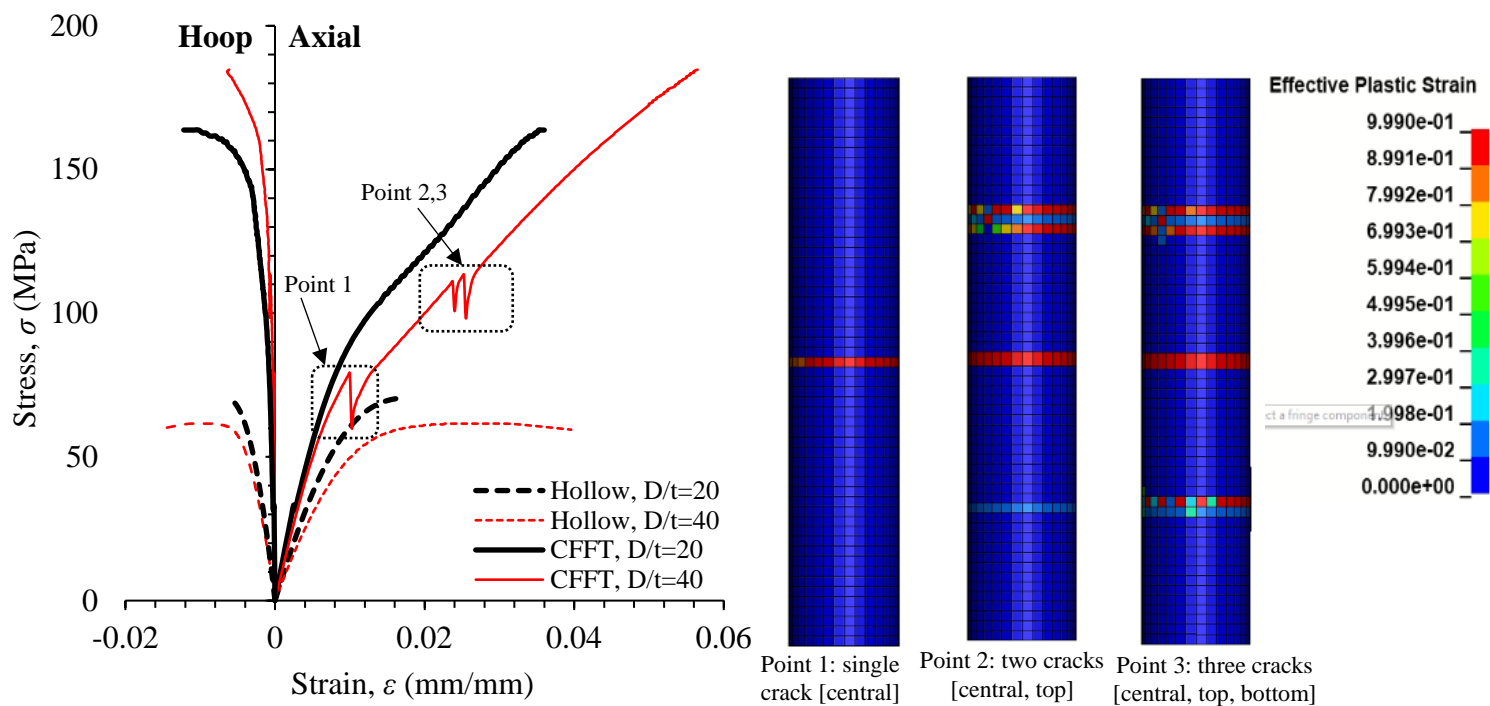
(a) Specimen FE-10 cracking (left) and intact tube at peak load (right)

Specimen	Key characteristics	Failure mode
FE-10	$\mu=0$, at failure (time=2 sec.)	
	$\mu=0.2$, at failure (time=2 sec.)	
	$\mu=0.3$, at failure (time=2 sec.)	
FE-11	$\mu=0.2$, at failure (time=2 sec.)	

μ = friction coefficient.

(b) Sensitivity analysis of friction coefficient

Figure 8. FE simulation of failure modes in concrete-filled $\pm 55^\circ$ GFRP tube specimens.



(a) Stress-strain curves. (b) Concrete cracking in specimen (FE-11) with ($D/t = 40$).

Figure 9. Comparing behavior of $\pm 55^\circ$ GFRP tube, hollow and CFFT specimens.

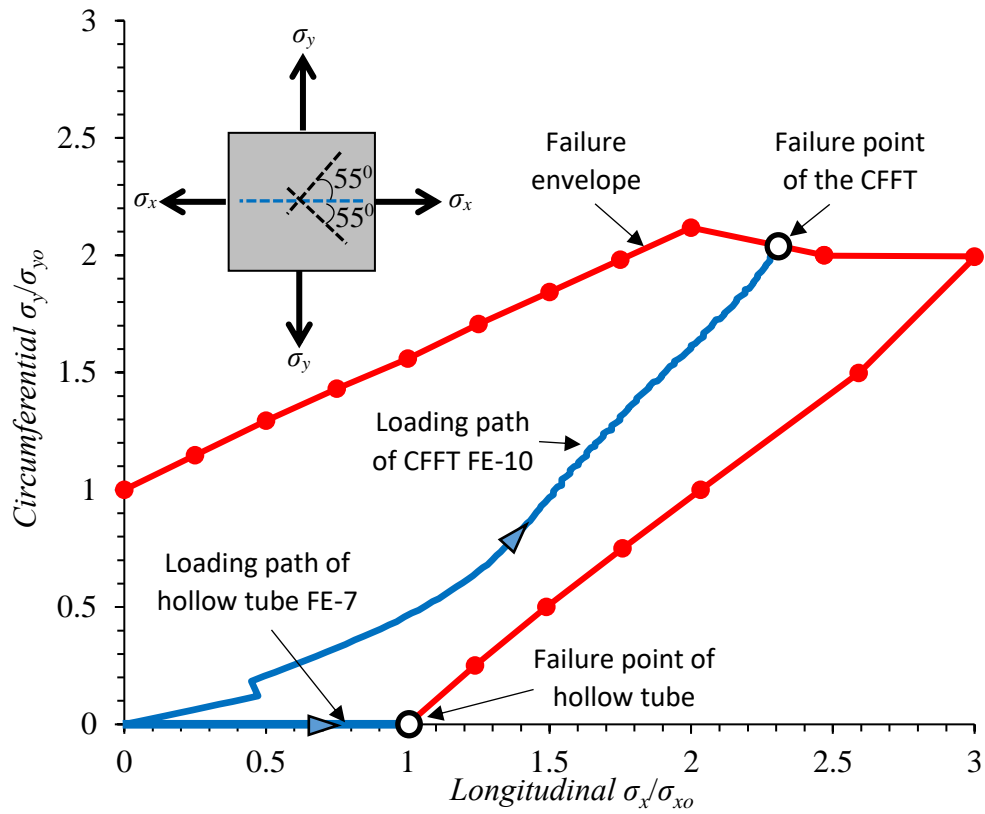


Figure 10. Effects of biaxial tension-tension stress state on axial strength (σ_{max}) of $\pm 55^\circ$ GFRP tube of FE-10.

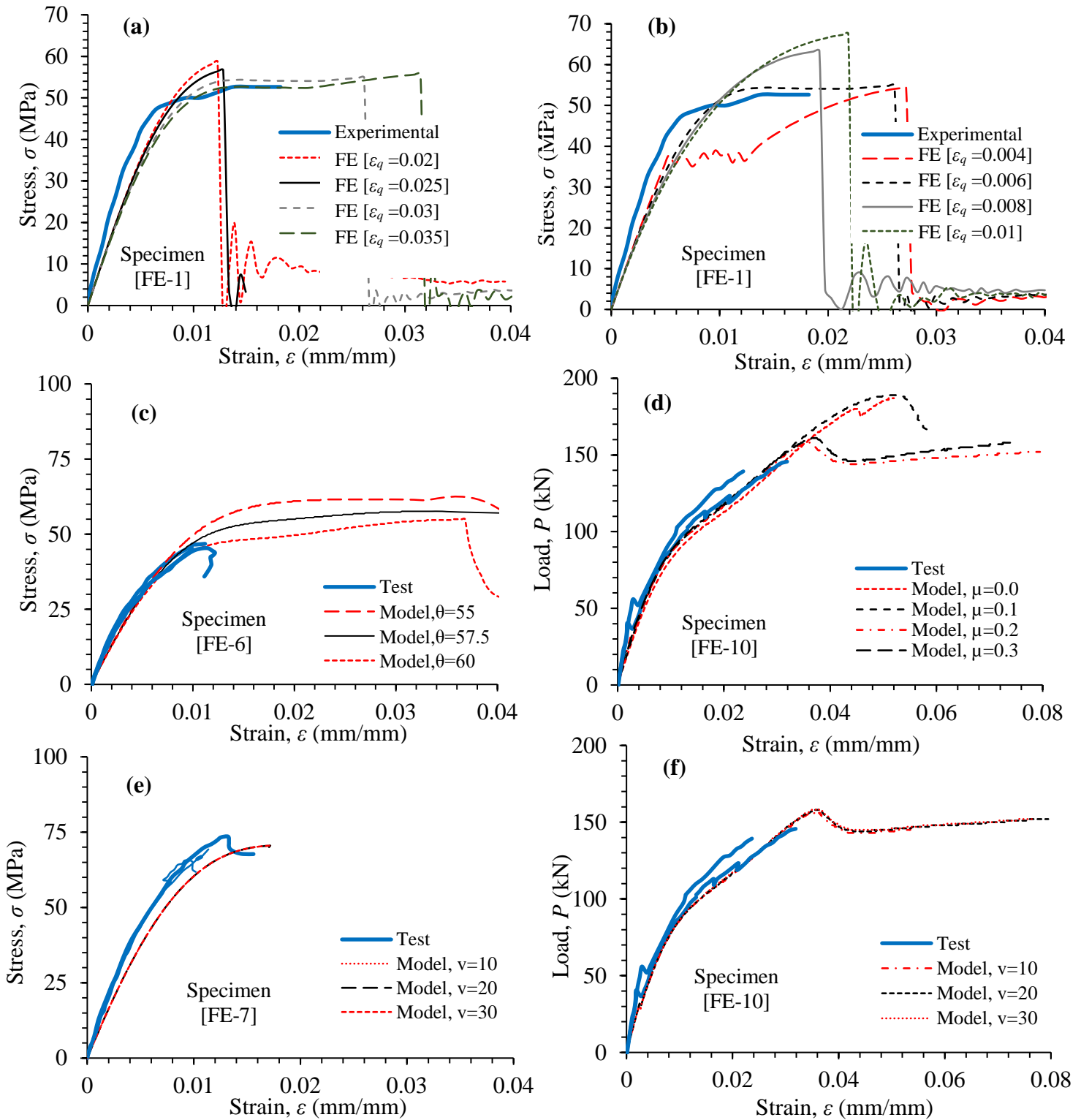


Figure 11. Results of sensitivity analyses: (a) and (b) effect of ultimate strain for in-plane shear and transverse tension, respectively; (c) effect of winding angle; (d) effect of friction coefficient; (e) and (f) effect of loading velocity in hollow and CFFT tubes, respectively.

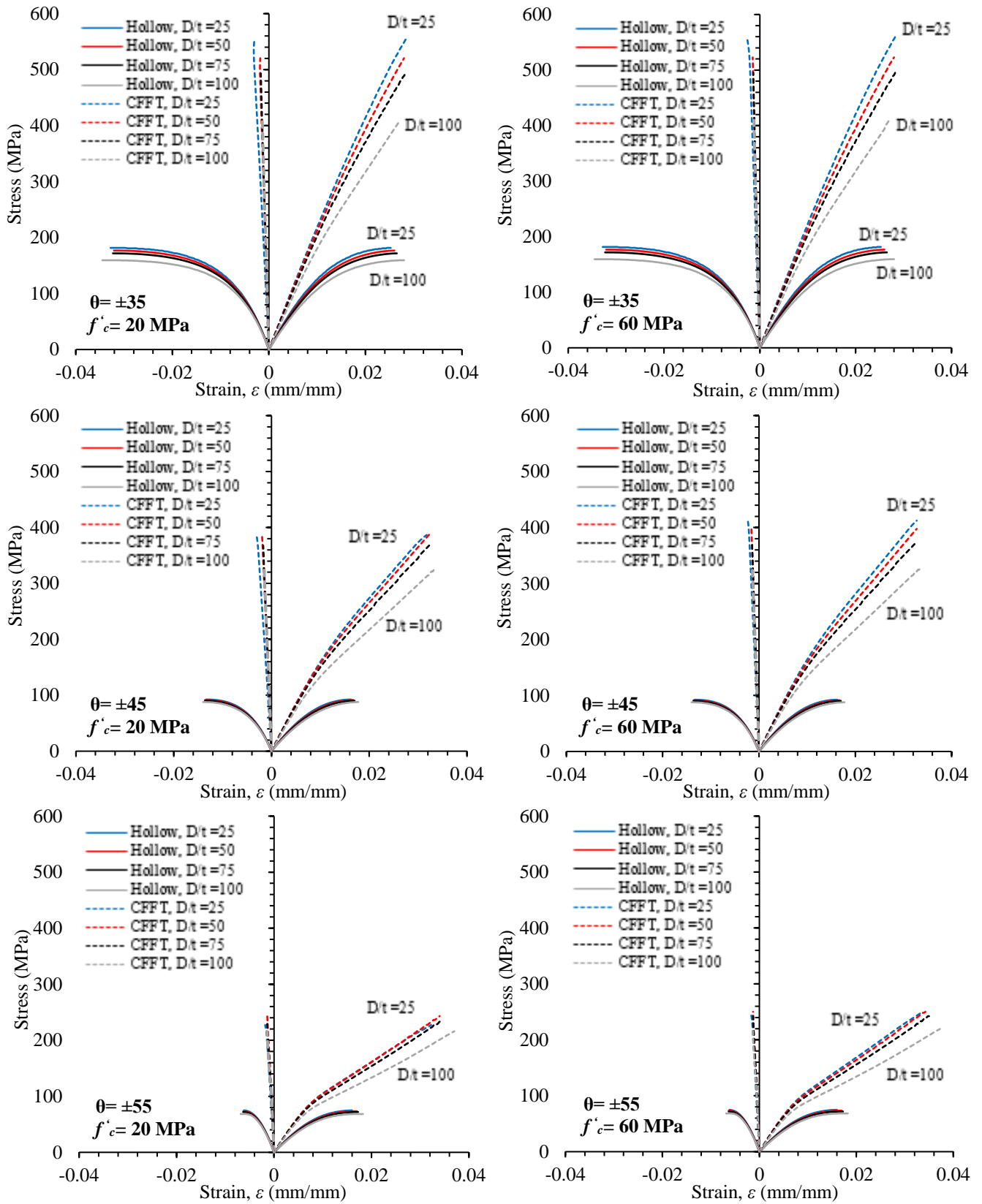


Figure 12. Tensile stress-strain curves in hollow and concrete-filled $\pm \theta^\circ$ GFRP tubes, for different winding angles (θ), D/t ratios, and concrete strengths (f'_c).

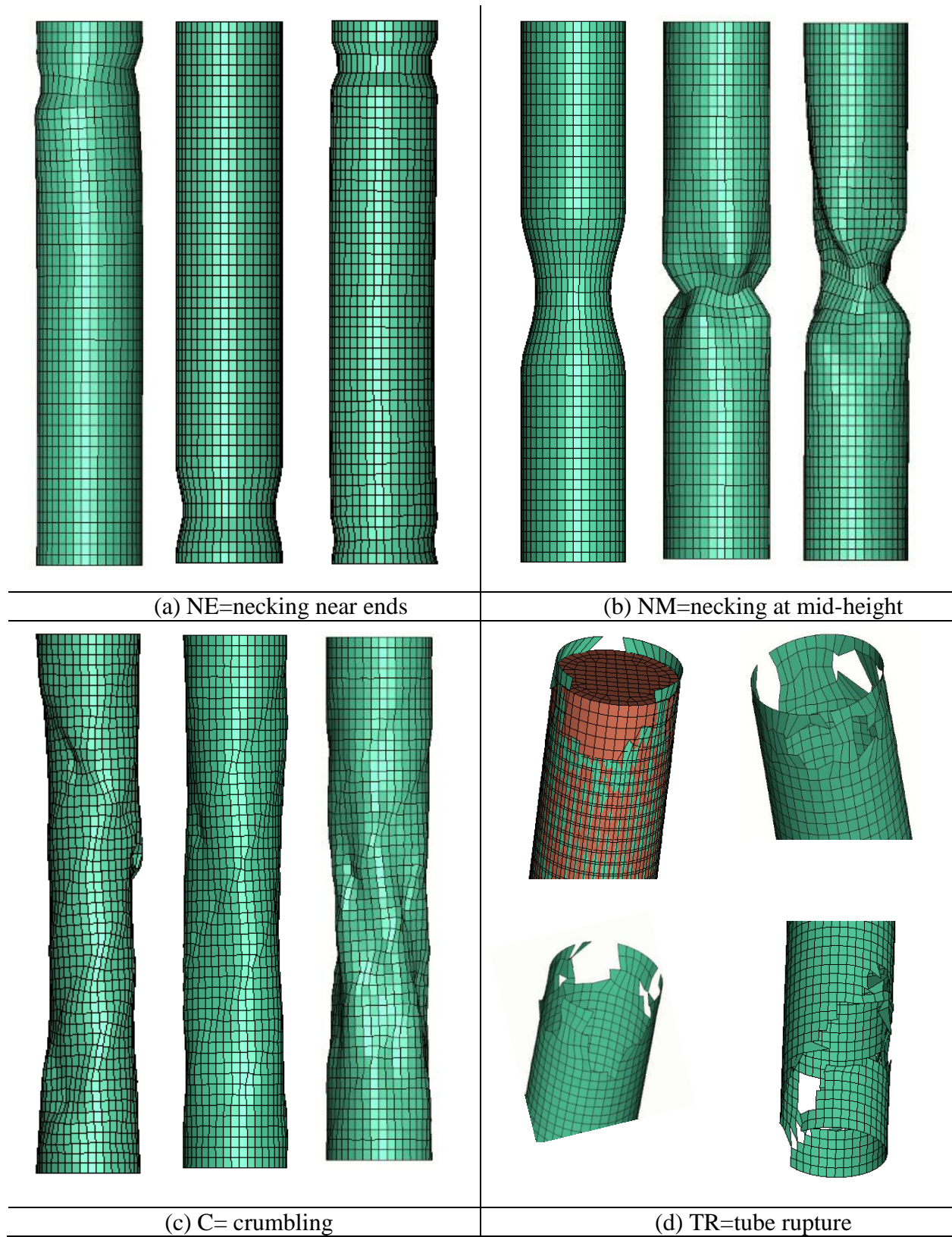
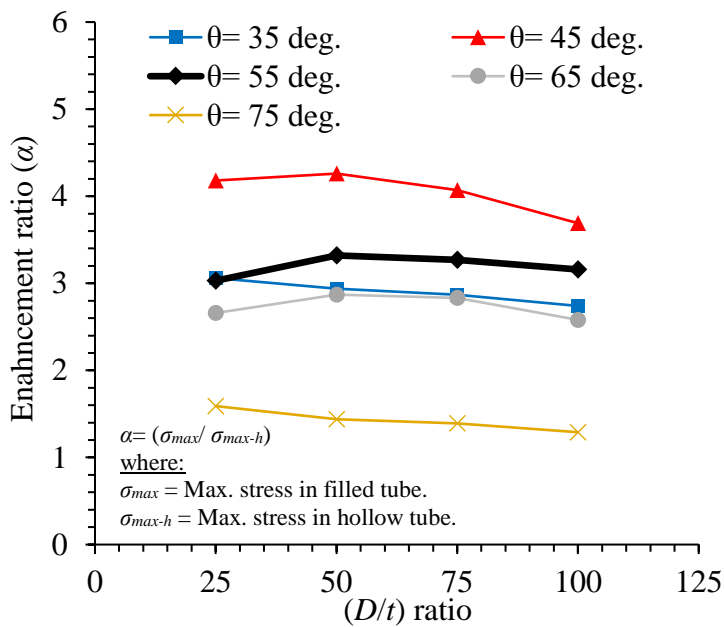
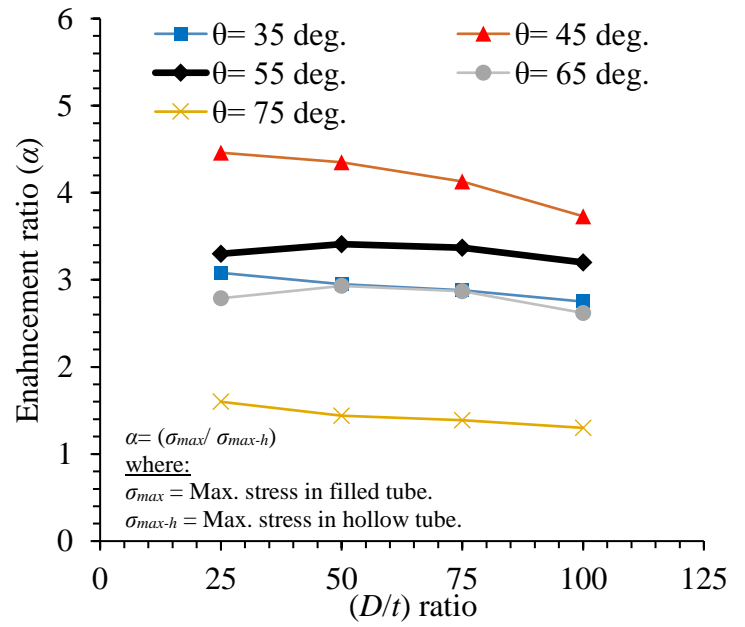


Figure 13. Failure modes observed in parametric study, in hollow and concrete-filled tubes.

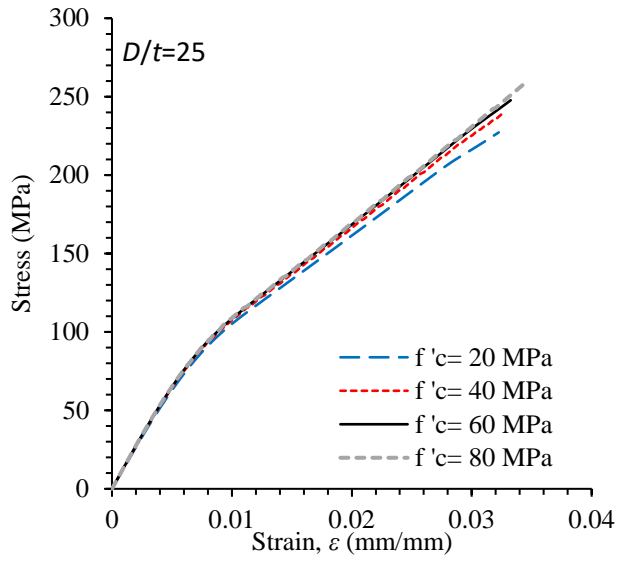


(a) $f'_c = 20$ MPa

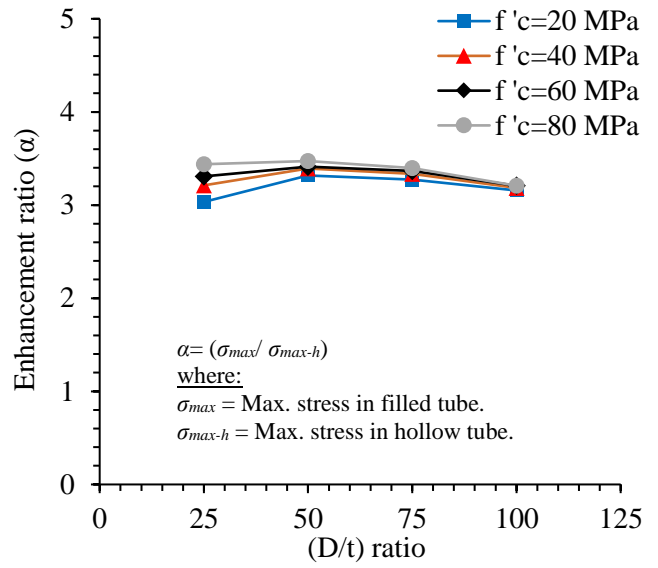


(b) $f'_c = 60$ MPa

Figure 14. Stress enhancement ratio (α) for concrete-filled $\pm\theta^\circ$ GFRP tubes, with different winding angles (θ), D/t ratios, and concrete strengths (f'_c).

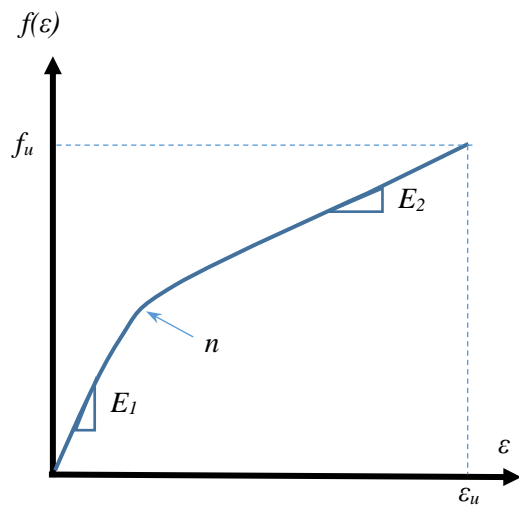


(a) Stress-strain curves.

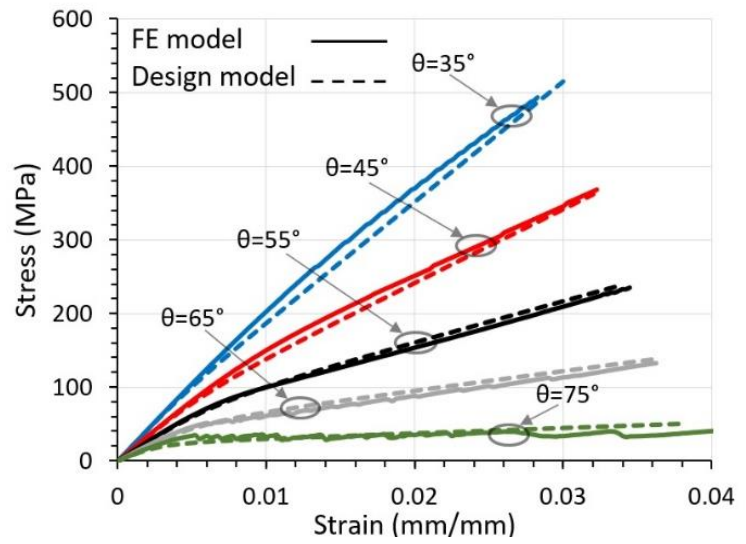


(b) α ratio vs. D/t ratio

Figure 15. Effects of concrete strengths (f'_c) on tensile stress-strain curves of concrete-filled $\pm 55^\circ$ GFRP tubes.



(a)



(b)

Figure 16. Design-oriented model: (a) General expression of the stress-strain behavior of angle-ply tube of a CFFT, and (b) Performance of the design-oriented model against the FE model.

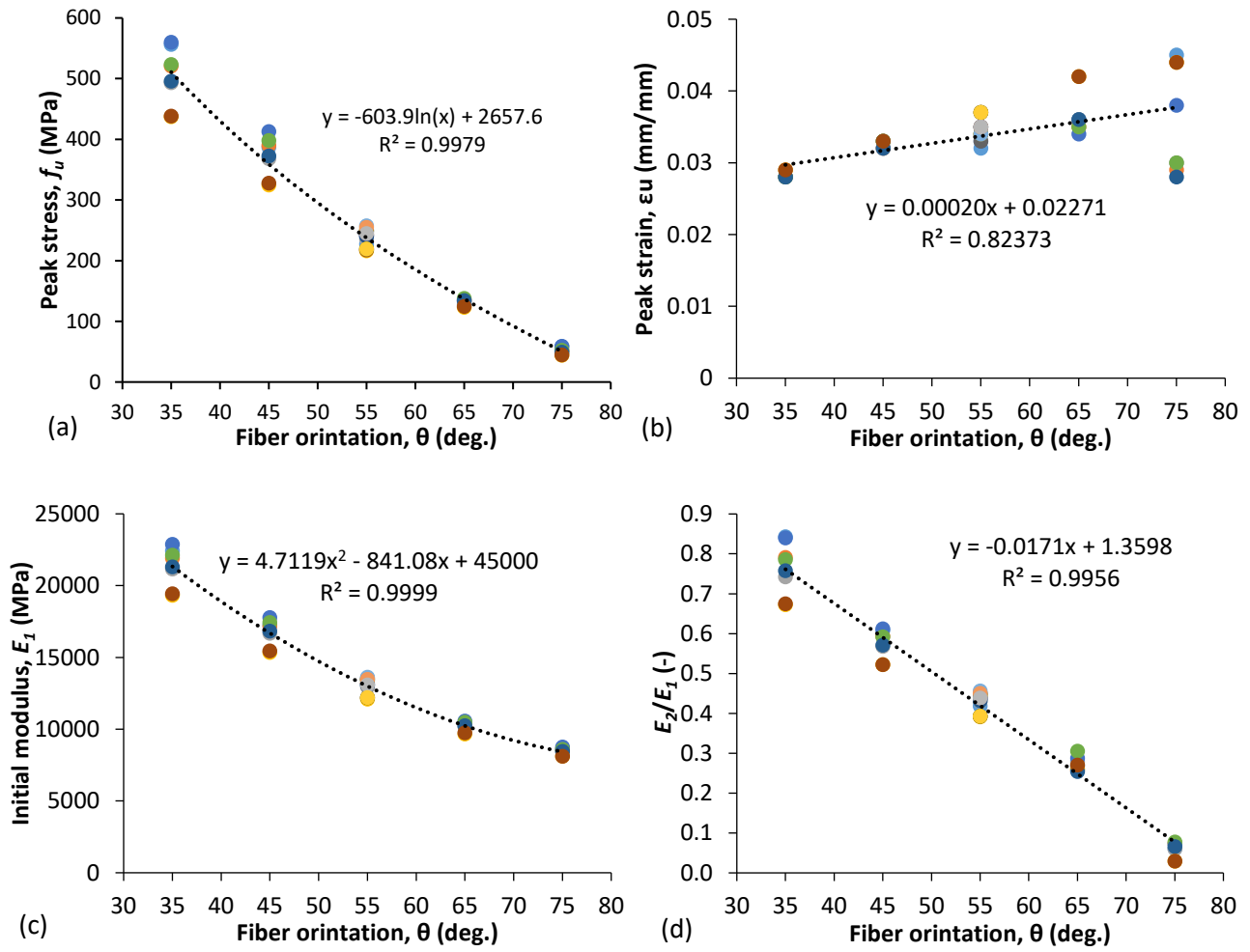


Figure 17. Calibration of main parameters for proposed design-oriented equation: (a) peak stress; (b) peak strain; (c) initial modulus; and (d) secondary modulus.